Experimental design and performance optimization of an AR-guided hybrid cutting guide for mandibular resection

Federico Salerno[1 (✉) [0000-0001-5282-9513]], Luca Ulrich[1 [0000-0001-8407-0660]], Giorgia Marullo[1 [0000-0002-2359-4409]], Emanuele Zavattero[2 [0000-0002-2758-6406]], Guglielmo Ramieri[2 [0000-0002-3131-9669]], Sandro Moos[1 [0000-0001-5097-7344]], and Enrico Vezzetti[1 [0000-0001-8910-7020]]

[1] Department of Management and Production Engineering, Politecnico di Torino, 10129 Torino, Italy
[2] Department of Surgical Sciences, Università degli Studi di Torino, 10126 Torino, Italy
federico.salerno@polito.it

Abstract. The use of surgical cutting guides for mandibular osteotomies is a consolidated approach in maxillo-facial surgery, typically based on patient-specific designs relying on anatomical fitting. However, these solutions may be limited by intraoperative variability and reduced flexibility. This study proposes and experimentally investigates an AR-guided hybrid cutting guide combining a physical constraint with augmented reality support for guide positioning and alignment. A full-factorial Design of Experiments was defined to evaluate the influence of key design parameters on system performance, including the tracking modality for pose estimation (marker), the adjustment strategy of the guide (adjustment), and the type of physical constraint provided to the cutting instrument (guide). A total of 27 configurations were tested with 40 replications each on mockups replicating irregular bone-like surfaces, considering geometric deviation, quantified through the Hausdorff distance between the planned cutting profile and the executed cut, and total task time as response variables. The results show that the configuration combining a cubic marker, rigid adjustment, and linear guide provides the best performance, while more complex adjustment strategies and geometries lead to increased variability and execution time. A desirability-based multi-response optimization confirmed this configuration as the optimal solution, with a global desirability index outperforming all alternatives.

Keywords: Augmented reality · Surgical guides · Computer-assisted surgery · Maxillofacial surgery · Pose estimation

1 Introduction

In cranio-maxillofacial surgery, surgical cutting guides support osteotomies, bone repositioning, and distraction procedures [18], constraining the instrument along predefined trajectories to transfer the preoperative plan to the operative field [15] with high precision and repeatability [21]. In clinical practice they are typically patient-specific, designed from preoperative Computed Tomography (CT) data [11] and replicating the patient anatomy for stable positioning through geometric fitting [5]. Despite their effectiveness, patient-specific guides present relevant limitations [17]: their performance depends on the consistency between preoperative imaging and intraoperative conditions [9], anatomical changes or limited bone exposure due to soft tissues may compromise fitting accuracy or prevent correct placement [4], and stable fitting often requires large contact surfaces, leading to invasive designs that increase surgical complexity and reduce flexibility [20]. To address these issues, this work proposes a hybrid cutting guide combining a physical structure with an augmented reality (AR) module: the physical component provides mechanical guidance, while AR supports positioning and alignment with respect to the planned osteotomy through visual feedback [19], with tracking markers enabling real-time pose estimation within the AR environment [7, 14]. Although developed for mandibular surgery, the concept is extendable to other anatomical regions. Within this framework, the study systematically investigates different design configurations of the proposed system, varying key parameters related to guide structure, adjustment strategy, and tracking modality, to identify the configuration that optimizes overall system efficiency in terms of both geometric performance and practical usability. The remainder of the paper is organized as follows. Section 2 describes the materials and methods, Section 3 presents the results, and Section 4 discusses the findings and concludes the paper.

2 Materials and methods

2.1 Hybrid cutting guide overview

The proposed system integrated two coordinated components, a physical module providing mechanical guidance and an AR-based module providing visual feedback during positioning. An overview is given in Fig. 1 (left), showing the pose estimation of the guide relative to the Head-Mounted Display (HMD) and the corresponding transformation. The physical module (Fig. 1, right) consisted of a base structure with three contact elements, ensuring stable support even on irregular anatomical surfaces without requiring full anatomical fitting, while a cutting guide element constrained the surgical instrument so that the blade followed the intended trajectory through direct mechanical contact. A removable tracking marker could be inserted into a dedicated slot. The AR module used a Microsoft HoloLens 2 as HMD: a dedicated Unity-based application visualized the target pose [13] as a virtual hologram superimposed onto the surgical scene and provided real-time feedback on the deviation between the current and target pose during manual positioning. The target pose was defined with respect to the planned osteotomy and anchored to the surgical scene through an image target rigidly referenced to the specimen support, which established a common reference frame between the preoperative plan and the physical setup. During execution, the HoloLens 2 continuously tracked the marker integrated in the guide to estimate its pose, and the residual deviation with respect to the target pose was computed and displayed to guide manual alignment.

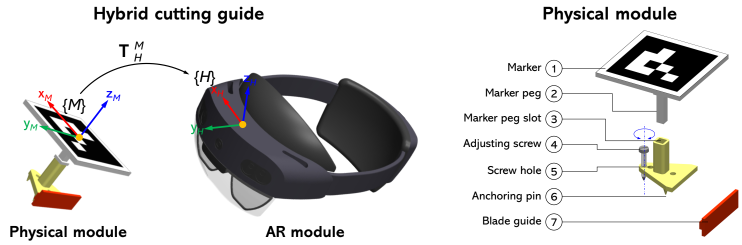

Fig. 1. Overview of the hybrid cutting guide. Left: system representation with guide pose estimation relative to the HMD. Right: exploded view of the physical module and its main components.

2.2 Experimental setup

A full-factorial Design of Experiments (DOE) [16] was defined to investigate the influence of key design parameters on the performance of the proposed AR-guided hybrid cutting guide for mandibular resection. The design included three categorical factors, each evaluated at three levels, resulting in a 3^3 scheme with 27 configurations, schematically shown in Fig. 2. Factor A (Marker) defined the AR

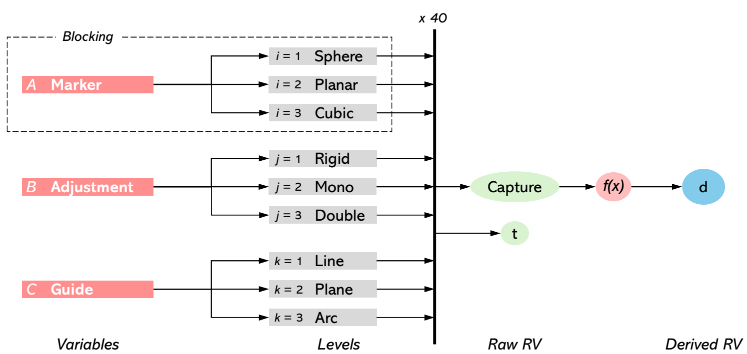

Fig. 2. Full-factorial DOE scheme with factors Marker (A), Adjustment (B), and Guide (C), each evaluated at three levels, and associated response variables.

tracking modality, with spherical, planar, and cubic configurations determining the pose estimation strategy. Factor B (Adjustment) described the mechanism used to stabilize the guide on the specimen after AR-based positioning. In the *rigid* configuration the guide had no adjustment element and was placed as a single fixed body, relying entirely on its three contact points. The *mono* configuration added a single adjustable anchoring element, providing one degree of freedom to compensate for residual misalignment after placement, whereas the *double* configuration introduced two anchoring elements, and thus two degrees of freedom, allowing finer local adaptation to the surface at the cost of a more articulated alignment procedure. Factor C (Guide) represented the geometry of the cutting constraint, with line, plane, and arc configurations. All 27 combinations were shown in Fig. 3. The experimental task consisted of positioning the

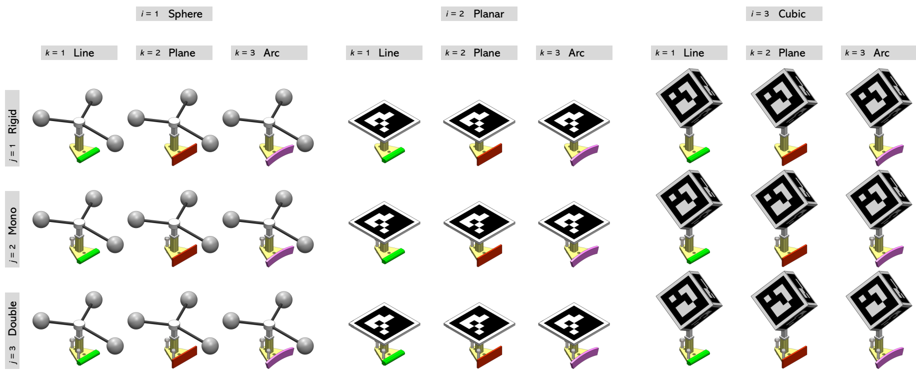

Fig. 3. All 27 combinations of the factor levels A, B, and C, corresponding to the implemented cutting guide configurations.

guide using AR, stabilizing it through the selected adjustment configuration, and performing the cut with a piezoelectric surgical handpiece (Aesculap GBL30R) constrained by the physical guide. Each trial was performed on a randomly generated irregular surface simulating generic bone geometry without symmetries. Specimens were manufactured in expanded polyurethane foam via molding, enabling rapid fabrication with sufficient geometric variability. Each specimen also included scale-reference holes located at the vertices of a 45 mm square and arranged in a regular grid, providing an in-image metric reference for the pixel-to-millimetre conversion. For each configuration (A_i, B_j, C_k), with $i, j, k \in \{1, 2, 3\}$, 40 replicated trials were performed, resulting in 1080 observations. Each trial included guide positioning, stabilization, and cutting, and two response variables were considered. The experimental procedure was summarized in Fig. 4. The first response variable was the total task time, from guide positioning to cut execution; the second was a geometric metric derived from the comparison between the executed cut and the theoretical target. After each trial, the resulting cut was acquired using an 8 MP USB camera (SVPRO, IMX179 sensor, resolution 3264×2448) equipped with a 5-50 mm manual zoom lens, positioned above the specimen and rigidly mounted through a custom support of metal rods and 3D-printed fixtures (Fig. 4), ensuring a stable and repeatable acquisition. To allow the geometric error to be interpreted in physical units, the acquisition geometry was set so that the camera frame covered a region of approximately 130×100 mm at a camera-to-specimen distance of about 280 mm, corresponding to horizontal and vertical fields of view of roughly 26° and 20°. Combined with the sensor resolution of 3264×2448 px and the scale-reference holes present on each specimen, this yielded a conversion factor of approximately 0.04 mm/px, which, given the fixed acquisition geometry, applied uniformly to all reported measurements. The

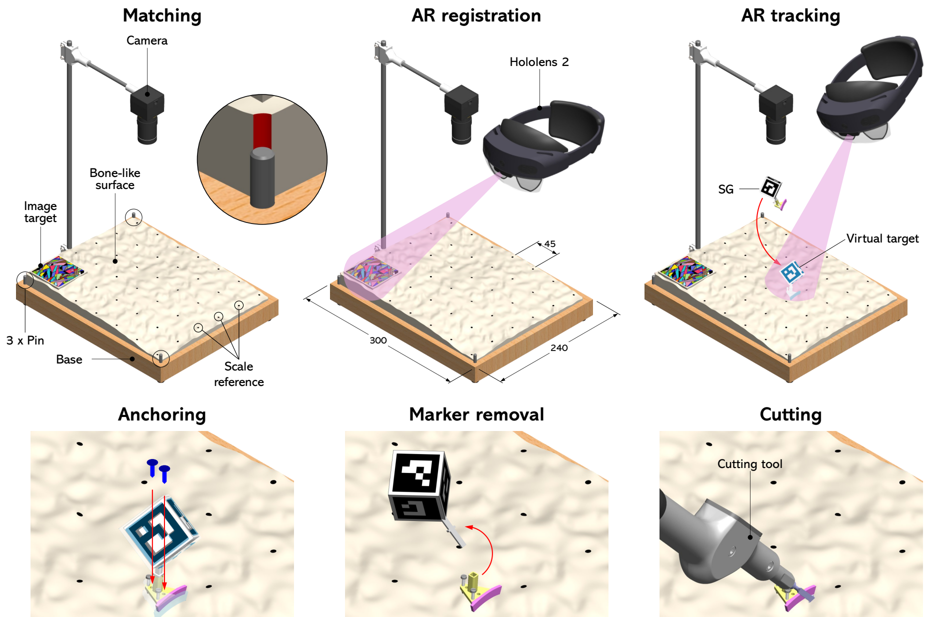

Fig. 4. Overview of the experimental procedure, including guide positioning, cutting execution, and post-processing for accuracy evaluation.

acquired images were processed to extract the silhouette of the executed cut, which was then geometrically aligned with the reference ground truth, defined as the ideal straight cutting path, through a planar registration procedure. Custom models were designed in SolidWorks (Dassault Systèmes®, France) and the tracking algorithms developed in Unity (Unity Technologies, USA; v2022.3.28f1); physical components were fabricated by fused filament fabrication (FDM) on a Creality K1C 3D printer (Creality®, China) using polylactic acid (PLA). The geometric error d was quantified using the Hausdorff distance [8, 12], a robust measure of the maximum discrepancy between two sets of points, computed here between the planned and executed cutting profiles. A schematic representation of the distance computation is shown in Fig. 5. Given two subsets A and B of a metric space, the Hausdorff distance was defined as:

$$d = d_H(A, B) = \max \left\{ \sup_{a \in A} \left[\inf_{b \in B} \|a - b\| \right], \sup_{b \in B} \left[\inf_{a \in A} \|a - b\| \right] \right\} \qquad (1)$$

In the specific case of cutting profile comparison, A represented the theoretical cutting profile, while B denoted the extracted profile from the executed cut, both defined in the two-dimensional image domain. To formally relate the design factors to the observed responses, a factorial model was adopted, in which each observation could be expressed as:

$$Y_{ijkl} = \mu + A_i + B_j + C_k + (AB)_{ij} + (AC)_{ik} + (BC)_{jk} + (ABC)_{ijk} + \varepsilon_{ijkl} \qquad (2)$$

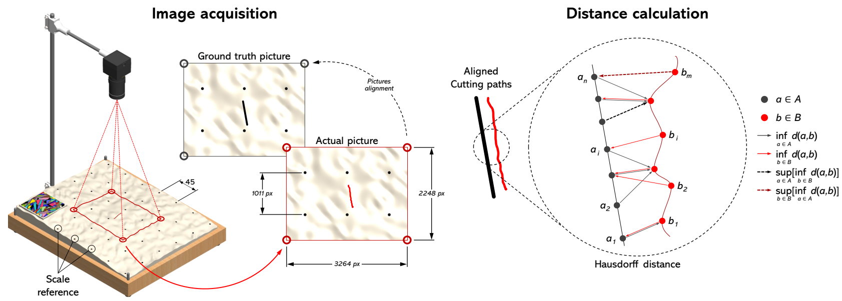

Fig. 5. Schematic representation of the geometric error computation. Left: acquisition of the executed cut, showing the scale-reference holes (vertices of a 45 mm square) and the image dimensions in pixels, together with the extraction of the corresponding path line. Right: detail of the Hausdorff distance calculation between the extracted cutting path and the theoretical ground truth profile.

where Y_{ijkl} denoted the observed response for the l-th replication under the factor-level combination (A_i, B_j, C_k), with $i, j, k \in \{1, 2, 3\}$ and $l = 1, \ldots, 40$. The term μ represented the overall mean, while A_i, B_j, and C_k corresponded to the main effects of Marker, Adjustment, and Guide, respectively. The terms $(AB)_{ij}$, $(AC)_{ik}$, and $(BC)_{jk}$ represented the two-way interaction effects, $(ABC)_{ijk}$ the three-way interaction, and ε_{ijkl} the residual variability. The model was fitted separately to the two responses, the Hausdorff distance d and the task time t.

3 Results

3.1 Descriptive analysis of experimental results

A total of 1080 observations were analyzed. Table 1 reports the descriptive statistics (mean and standard deviation of d and t) for the 27 experimental configurations. The lowest mean distance was observed for the configuration Planar-

Table 1. Descriptive statistics for all experimental conditions. Mean ± standard deviation of distance d (px) and time t (min) for each combination of Marker (i), Adjustment (j), and Guide (k). Distances in pixels can be converted to millimetres through the conversion factor reported in Section 2 ($\approx$ 0.04 mm/px).

		$i = 1$		$i = 2$		$i = 3$	
		d / px	t / min	d / px	t / min	d / px	t / min
$j = 1$	$k = 1$	15.5 ± 3.5	1.7 ± 0.5	11.2 ± 2.0	1.2 ± 0.3	11.3 ± 3.5	1.1 ± 0.2
	$k = 2$	17.1 ± 2.5	1.6 ± 0.4	13.4 ± 2.4	1.5 ± 0.4	12.0 ± 3.0	1.4 ± 0.3
	$k = 3$	16.7 ± 2.6	1.7 ± 0.4	18.2 ± 3.6	1.6 ± 0.4	14.5 ± 2.9	1.6 ± 0.4
$j = 2$	$k = 1$	14.1 ± 2.3	1.7 ± 0.4	17.0 ± 4.3	1.7 ± 0.5	16.2 ± 1.9	1.7 ± 0.4
	$k = 2$	14.7 ± 3.9	1.4 ± 0.3	16.9 ± 4.7	1.8 ± 0.5	16.5 ± 4.4	1.5 ± 0.4
	$k = 3$	14.3 ± 2.4	1.5 ± 0.3	17.2 ± 5.0	1.8 ± 0.5	19.5 ± 4.0	1.7 ± 0.4
$j = 3$	$k = 1$	14.4 ± 2.5	1.5 ± 0.4	14.7 ± 3.8	1.3 ± 0.3	16.6 ± 4.1	1.6 ± 0.4
	$k = 2$	15.1 ± 4.1	1.6 ± 0.4	16.6 ± 3.5	1.8 ± 0.4	17.8 ± 3.0	1.8 ± 0.3
	$k = 3$	15.4 ± 2.6	1.6 ± 0.4	17.8 ± 3.2	1.9 ± 0.4	21.9 ± 5.4	2.2 ± 0.5

Rigid-Line (11.2 px, $\approx$ 0.45 mm), and the highest for Cubic-Double-Arc (21.9 px, $\approx$ 0.88 mm); a similar trend held for the task time, from about 1.1 to over

2.2 min. The distributions in Fig. 6 show that the *Rigid* adjustment generally yielded lower distances and reduced variability, particularly for the Line configuration, whereas the *Double* condition produced larger dispersion and higher values, especially with the Arc guide. The marker effect was less pronounced, although the Planar configuration tended to yield lower values in several conditions. Interaction effects were also observed, as shown in Fig. 7: the increase

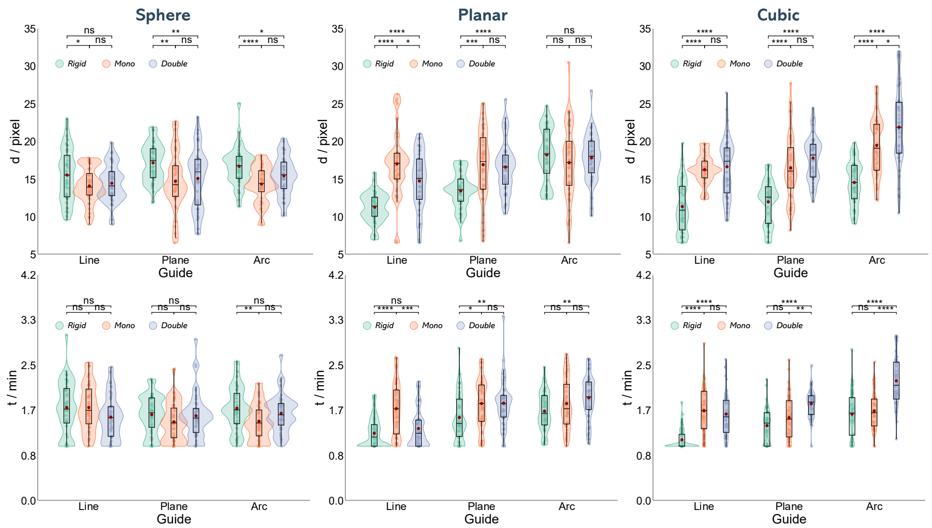

Fig. 6. Distribution of distance d (top) and time t (bottom) across guide geometries and adjustment strategies for each marker type.

in distance from Line to Arc was more pronounced for the Double adjustment, while the Rigid configuration behaved more stably across guides, and a comparable pattern held for the task time, confirming the Adjustment–Guide interaction.

3.2 Factorial model analysis

The factorial model of Eq. 2 was fitted to the two responses to assess the contribution of the factors and their interactions; the ANOVA results are reported in Table 2. For the distance d, all main effects were significant, with Guide contributing most, followed by Adjustment and, to a lesser extent, Marker; all two-way and the three-way interactions were significant as well, indicating that each factor's effect on geometric performance depended on the levels of the others. For the time t, Adjustment and Guide were the dominant main effects while Marker was not significant; all two-way interactions were significant but the three-way interaction was not, suggesting that procedural time was mainly driven by pairwise factor effects rather than by a higher-order combined effect.

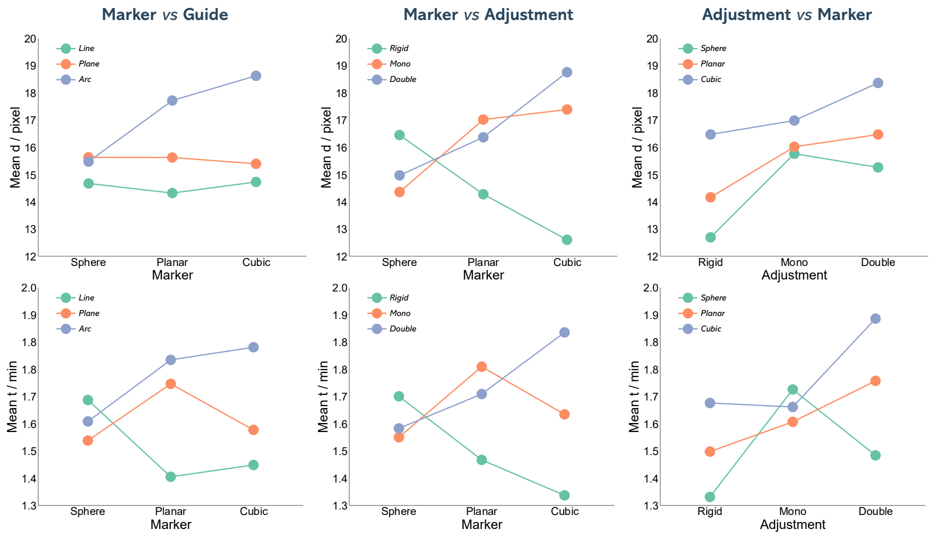

Fig. 7. Interaction plots of mean distance d (top) and time t (bottom) across combinations of Marker, Adjustment, and Guide factors.

Table 2. ANOVA results for the response variables distance d and time t based on the factorial model in Eq. 2. Factors are denoted as A (Marker), B (Adjustment), and C (Guide).

Effect	Distance d			Time t		
	F	p-value	η_p^2	F	p-value	η_p^2
A	7.41	0.00064	0.014	1.02	0.360	0.002
B	42.11	< 0.001	0.074	24.04	< 0.001	0.044
C	55.10	< 0.001	0.095	27.38	< 0.001	0.049
$A \times B$	46.05	< 0.001	0.149	21.60	< 0.001	0.076
$A \times C$	9.57	< 0.001	0.035	14.49	< 0.001	0.052
$B \times C$	4.34	0.0017	0.016	11.90	< 0.001	0.043
$A \times B \times C$	3.78	< 0.001	0.028	0.84	0.569	0.006

3.3 Multi-response optimization of the design configuration

A multi-response optimization was then performed to identify the configuration providing the best trade-off between geometric accuracy and procedural efficiency, jointly minimizing the plane distance error d and the task time t. Because the factors were categorical, the optimum was sought among the finite set of tested factor-level combinations rather than over a continuous parameter space. Let

$$\Omega = \{(A_i, B_j, C_k) \mid i, j, k \in \{1, 2, 3\}\} \tag{3}$$

denote the set of all feasible design configurations, with cardinality $|\Omega| = 27$. For each configuration $\omega \in \Omega$, the replicated observations were synthesized through the sample means of the two responses,

$$\bar{d}(\omega) = \frac{1}{n} \sum_{l=1}^{n} d_l(\omega), \qquad \bar{t}(\omega) = \frac{1}{n} \sum_{l=1}^{n} t_l(\omega), \tag{4}$$

with $n = 40$ replications per condition. Because the two responses have different units and ranges, each was transformed into an individual desirability function ranging from 0 (least desirable) to 1 (most desirable). Since both responses had to be minimized, a generic variable v (either d or t) is introduced, and the desirability was defined according to a smaller-the-better criterion as

$$D_v(\omega) = \frac{\max_{\omega \in \Omega} \bar{v}(\omega) - \bar{v}(\omega)}{\max_{\omega \in \Omega} \bar{v}(\omega) - \min_{\omega \in \Omega} \bar{v}(\omega)}, \tag{5}$$

so that lower values of $\bar{v}(\omega)$ correspond to higher desirability. The overall performance of each configuration was then quantified through a global desirability index, the geometric mean of the two individual desirabilities:

$$D(\omega) = \left[D_d(\omega)\, D_t(\omega)\right]^{1/2}, \tag{6}$$

and the optimal configuration ω^* was identified as

$$\omega^* = \arg\max_{\omega \in \Omega} D(\omega). \tag{7}$$

The formulation was applied to all 27 configurations to compute desirability scores and derive a global ranking, summarized in Fig. 8, where configurations closer to the upper-right region combine low geometric deviation and reduced task duration. The configuration A_3-B_1-C_1 achieved the highest global desirability, i.e., the most balanced performance across the two responses, despite not minimizing the distance metric alone.

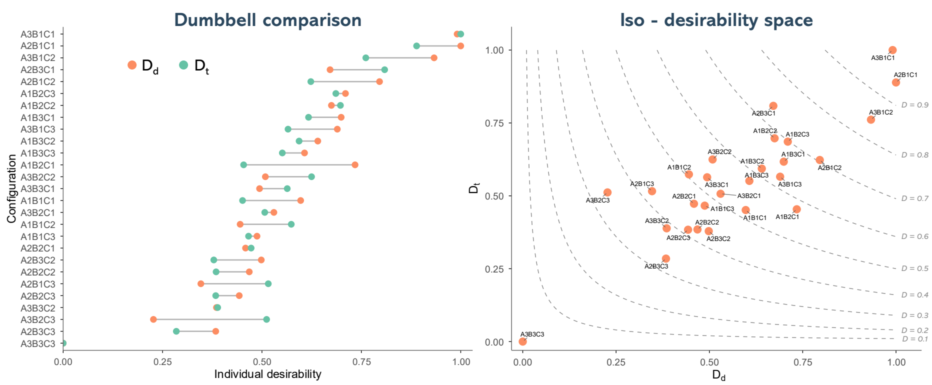

Fig. 8. Desirability-based analysis of the 27 configurations. Left: dumbbell plot of individual desirability scores for distance (D_d) and time (D_t). Right: scatter plot in the desirability space with iso-desirability curves. Configuration labels follow (A_i, B_j, C_k), where subscripts denote factor levels as defined in Fig. 2.

4 Discussion and conclusions

The most effective configuration combined a cubic marker with ArUco patterns, a rigid guide without adjustment mechanisms, and a linear cutting constraint, achieving the best trade-off between geometric accuracy and total procedural time. The cubic marker's multi-face geometry improved pose-estimation robustness across viewing angles, whereas planar markers suffered from visibility and orientation bias [3] and spherical markers from depth-sensing limitations [10]; although the planar marker gave the lowest mean distance in one specific condition, its higher variability across configurations lowered its overall desirability. Rigid configurations reduced interaction complexity and operator-induced variability, while adjustable mechanisms increased alignment effort, and the linear guide offered a stable constraint with limited rotational freedom for minor compensatory adjustments during cutting. Overall, system performance was driven mainly by the interaction between mechanical design and AR support rather than by tracking accuracy alone: AR was effective only when coupled with a simple and stable physical structure, whereas increasing mechanical complexity reduced robustness, so that constraining the system through minimal, well-defined degrees of freedom emerged as a key factor for reliable AR-assisted workflows. These findings complement previous studies on patient-specific guides, which emphasize anatomical fitting for accuracy [18], and AR-based systems focusing on visualization and registration [22]; compared to approaches prioritizing tracking performance [6], mechanical stability and interaction simplicity had a stronger impact on overall performance, in line with recent studies highlighting the importance of usability and system integration in AR-guided procedures [2]. From a clinical standpoint, a hybrid guide requiring minimal intraoperative adjustment could reduce setup complexity and the operator effort associated with alignment while preserving the accuracy transfer typical of physical guides; in mandibular reconstruction, the reduced reliance on large anatomical contact surfaces may also enable less invasive and more flexible designs. Several limitations should nonetheless be acknowledged before clinical translation. First, registration here relied on an image target rigidly referenced to the mock-up, whereas in a real scenario such fiducials may not be available on the exposed bone, requiring alternative strategies (e.g., surface- or landmark-based registration, or bone-anchored fiducials) whose robustness must still be assessed. Second, the expanded polyurethane mock-ups reproduce irregular bone-like geometries but not the mechanical response of real bone to piezoelectric cutting, which may affect the generalizability of the measured deviations. Third, all trials were performed by a single operator, so inter-operator variability was not captured. Finally, the evaluation considered only geometric deviation and task time, leaving out clinically relevant factors such as soft-tissue interference, limited intraoperative visibility, patient-specific anatomical variability, cognitive workload, and user experience [1]. Future developments will address these aspects through an "outside-in" tracking approach, in which pose estimation is performed externally and visualized on the HMD to improve registration robustness, and through validation on anatomically realistic and, ultimately, ex vivo specimens, together with multi-operator user studies including workload, interaction quality, and usability metrics.

References

1. Andersen, D., Popescu, V., Cabrera, M.E., Shanghavi, A., Gomez, G., Marley, S., Mullis, B., Wachs, J.P.: Medical telementoring using an augmented reality transparent display. Surgery **159**(6), 1646–1653 (2016). https://doi.org/10.1016/j.surg.2015.12.016
2. Condino, S., Turini, G., Parchi, P.D., Viglialoro, R.M., Piolanti, N., Gesi, M., Ferrari, M., Ferrari, V.: How to build a patient-specific hybrid simulator for orthopaedic open surgery: benefits and limits of mixed-reality using the microsoft hololens. Journal of healthcare engineering **2018**(1), 5435097 (2018). https://doi.org/10.1155/2018/5435097
3. Jurado-Rodriguez, D., Muñoz-Salinas, R., Garrido-Jurado, S., Medina-Carnicer, R.: Planar fiducial markers: a comparative study. Virtual Reality **27**(3), 1733–1749 (2023). https://doi.org/10.1007/s10055-023-00772-5
4. Lee, S.H., Kim, W., Lee, J.S.: What are the resection accuracy and guide-fitting errors associated with 3d-printed, patient-specific resection guides for bone tumour resections? The bone & joint journal **105**(2), 190–197 (2023). https://doi.org/10.1302/0301-620X.105B2.BJJ-2022-0585.R2
5. Liu, Y.f., Xu, L.w., Zhu, H.y., Liu, S.S.Y.: Technical procedures for template-guided surgery for mandibular reconstruction based on digital design and manufacturing. Biomedical engineering online **13**(1), 63 (2014). https://doi.org/10.1186/1475-925X-13-63
6. Ma, L., Zhao, Z., Chen, F., Zhang, B., Fu, L., Liao, H.: Augmented reality surgical navigation with ultrasound-assisted registration for pedicle screw placement: a pilot study. International journal of computer assisted radiology and surgery **12**(12), 2205–2215 (2017). https://doi.org/10.1007/s11548-017-1652-z
7. Malhotra, S., Halabi, O., Dakua, S.P., Padhan, J., Paul, S., Palliyali, W.: Augmented reality in surgical navigation: a review of evaluation and validation metrics. Applied Sciences **13**(3), 1629 (2023). https://doi.org/10.3390/app13031629
8. Mamone, V., Ferrari, V., Condino, S., Cutolo, F.: Projected augmented reality to drive osteotomy surgery: Implementation and comparison with video see-through technology. IEEE access **8**, 169024–169035 (2020). https://doi.org/10.1109/ACCESS.2020.3021940
9. Martelli, N., Serrano, C., van den Brink, H., Pineau, J., Prognon, P., Borget, I., El Batti, S.: Advantages and disadvantages of 3-dimensional printing in surgery: A systematic review. Surgery (2016). https://doi.org/10.1016/j.surg.2015.12.017
10. Martin-Gomez, A., Li, H., Song, T., Yang, S., Wang, G., Ding, H., Navab, N., Zhao, Z., Armand, M.: Sttar: surgical tool tracking using off-the-shelf augmented reality head-mounted displays. IEEE Transactions on Visualization and Computer Graphics **30**(7), 3578–3593 (2023). https://doi.org/10.1109/TVCG.2023.3238309
11. Morrison, R.J., Hollister, S.J., Niedner, M.F., Mahani, M.G., Park, A.H., Mehta, D.K., Ohye, R.G., Green, G.E.: Mitigation of tracheobronchomalacia with 3d-printed personalized medical devices in pediatric patients. Science translational medicine **7**(285), 285ra64–285ra64 (2015). https://doi.org/10.1126/scitranslmed.3010825
12. Rockafellar, R.T., Wets, R.J.B.: Variational Analysis, Grundlehren der mathematischen Wissenschaften, vol. 317. Springer, Berlin, Heidelberg (1998). https://doi.org/10.1007/978-3-642-02431-3
13. Salerno, F., Contenti, A., Ulrich, L., Marullo, G., Moos, S., Vezzetti, E.: Mott modular optical tool tracking framework enabling efficient benchmarking. Sci Rep **15**(1), 37205 (2025). https://doi.org/10.1038/s41598-025-21044-z

14. Salerno, F., Contenti, A., Ulrich, L., Moos, S., Fiandrotti, A., Vezzetti, E.: A low-cost benchmarking platform for tracking systems to enable augmented surgery tools in clinical practice. SN Computer Science **7**(5), 437 (2026). https://doi.org/10.1007/s42979-026-05071-9
15. Salerno, F., Moos, S., Ulrich, L., Novaresio, A., Vezzetti, E.: A methodology for the dimensional and mechanical analysis of surgical guides. In: International Conference of the Italian Association of Design Methods and Tools for Industrial Engineering. pp. 184–193. Springer, Cham (2023). https://doi.org/10.1007/978-3-031-52075-4-22
16. Salerno, F., Ulrich, L., Maculotti, G., Moos, S., Genta, G., Vezzetti, E., Galetto, M.: A metrological approach for augmented reality tooltip tracking assessment. Computers in Industry **175**, 104430 (2026). https://doi.org/10.1016/j.compind.2025.104430
17. Salerno, F., Ulrich, L., Marullo, G., Moos, S., Vezzetti, E.: Advancing surgical cutting guide flexibility: a hybrid physical and augmented reality solution for cranio-maxillofacial surgery. Journal of Cranio-Maxillo-Facial Surgery (2026). https://doi.org/10.1016/j.jcms.2026.104480, in press
18. Tarsitano, A., Del Corso, G., Ciocca, L., Scotti, R., Marchetti, C.: Mandibular reconstructions using computer-aided design/computer-aided manufacturing: a systematic review of a defect-based reconstructive algorithm. Journal of Cranio-Maxillofacial Surgery **43**(9), 1785–1791 (2015). https://doi.org/10.1016/j.jcms.2015.08.006
19. Ulrich, L., Salerno, F., Moos, S., Vezzetti, E.: How to exploit augmented reality (ar) technology in patient customized surgical tools: a focus on osteotomies. Multimedia Tools and Applications pp. 1–32 (2024). https://doi.org/10.1007/s11042-023-18058-y
20. Unsal, G.S., Turkyilmaz, I., Lakhia, S.: Advantages and limitations of implant surgery with cad/cam surgical guides: A literature review. Journal of clinical and experimental dentistry **12**(4), e409 (2020). https://doi.org/10.4317/jced.55871
21. Van Assche, N., Van Steenberghe, D., Guerrero, M., Hirsch, E., Schutyser, F., Quirynen, M., Jacobs, R.: Accuracy of implant placement based on presurgical planning of three-dimensional cone-beam images: a pilot study. Journal of clinical periodontology **34**(9), 816–821 (2007). https://doi.org/10.1111/j.1600-051X.2007.01110.x
22. Vávra, P., Roman, J., Zonča, P., Ihnát, P., Němec, M., Kumar, J., Habib, N., El-Gendi, A.: Recent development of augmented reality in surgery: a review. Journal of healthcare engineering **2017**(1), 4574172 (2017). https://doi.org/10.1155/2017/4574172